DOI: 10.1002/chem.201001086

An Atomic-Level Strategy for Unraveling Gold Nanocatalysis from the Perspective of $Au_n(SR)_m$ Nanoclusters

Yan Zhu, Huifeng Qian, and Rongchao Jin*[a]

Abstract: An atomic-level strategy is devised to gain insight into the origin of nanogold catalysis by using atomically monodisperse $Au_n(SR)_m$ nanoclusters as well-defined catalysts for styrene oxidation. The $Au_n(SR)_m$ nanoclusters are emerging as a new class of gold nanocatalyst to overcome the polydispersity of conventional nanoparticle catalysts. The unique atom-packing structure and electronic properties of $Au_n(SR)_m$ nanoclusters (<2 nm) are rationalized to be responsible for their extraordinary catalytic activity observed in styrene oxidation. An interesting finding is that quantum size effects of $Au_n(SR)_m$ nanoclusters, rather than the higher specific surface area, play a major role in gold-catalyzed selective oxidation of styrene. For example, $Au_{25}(SR)_{18}$ nanoclusters (≈ 1 nm) are found to be particularly efficient in activating O_2, which is a key step in styrene oxidation, and hence, the ultrasmall Au_{25} catalyst exhibits higher activity than do larger sizes. This atomic-level strategy has allowed us to obtain an important insight into some fundamental aspects of nanogold catalysis in styrene oxidation. The ultrasmall yet robust $Au_n(SR)_m$ nanoclusters are particularly promising for studying the mechanistic aspects of nanogold catalysis and for future design of better catalysts with high activity and selectivity for certain chemical processes.

Keywords: atomic-level strategy · catalysis · gold · nanostructures · oxidation

Introduction

Gold nanoparticles have been demonstrated to exhibit catalytic activity in many chemical processes,[1–6] however, fundamental investigations on the structure–catalytic activity relationships still lag behind partly due to the polydispersity issue of gold nanoparticles; the latter also obscures the interesting size-dependent catalytic activity of nanogold and precludes an in-depth understanding of the origin of this size dependence. Moreover, identifying the catalytically active species in nanogold catalysis remains a major challenge due to the difficulty in attaining well-defined gold nanoparticles and solving their atomic structure, in particular the particle surface structure. Conventional Au nanoparticles, even the best quality colloidal nanoparticles, are still far from being well defined at the atomic level. The 2D or 3D model gold catalysts are certainly better defined, but the catalytic results obtained under high vacuum conditions are deviated from realistic systems, and hence, may not be directly transferable to real-world catalytic systems. In most cases, the structural polydispersity and heterogeneity of conventional nanocatalysts only give rise to an average ensemble of the catalytic performance. The attainment of atomic-level information on the nature of nanogold catalysis has been difficult.[7] Overall, the lack of atomically precise, well-defined nanogold systems has long been a major obstacle to pursuing fundamental studies on gold catalysis and to the development of efficient Au catalysts for wider catalytic applications.

Recently, atomically monodisperse, thiolate-capped Au nanoclusters (denoted as $Au_n(SR)_m$) have been successfully prepared and their catalytic properties have been demonstrated.[8–14] These well-defined catalysts hold promise as a new generation of nanogold catalysts and, more importantly, permit in-depth studies on the subtle correlation of structure and catalytic activity, since these nanoclusters are well defined and their structures start to be solved. Of note, in contrast to ligand-capped $Au_n(SR)_m$ nanoclusters, there have been numerous studies on ligand-removed Au_n nanoclusters or gas-phase Au_n deposited on supports for CO or alkene oxidation,[7,9,15,16] however, the atomic structures of the bare Au_n clusters are difficult to determine, albeit in some cases

[a] Dr. Y. Zhu, H. Qian, Prof. R. Jin
Carnegie Mellon University, Department of Chemistry
4400 Fifth Avenue, Pittsburgh, Pennsylvania 15213 (USA)
Fax: (+1) 412-268-1061
E-mail: rongchao@andrew.cmu.edu

Supporting information for this article is available on the WWW under http://dx.doi.org/10.1002/chem.201001086.

it can be inferred from spectroscopic studies in combination with DFT calculations. In the absence of the exact atomic structure, the interpretation of the catalytic performance is sometimes not complete and structure–property correlations cannot be attained.

We have developed wet-chemistry approaches for synthesizing well-defined Au_{25}, Au_{38}, and Au_{144} nanoclusters capped by phenylethanethiolate.[10–12] Herein, we explore their catalytic properties with a focus on the size-dependent effects in selective oxidation of styrene. The experimentally determined or theoretically computed structures of these $Au_n(SR)_m$ nanoclusters allow us to gain deep insight into their catalytic properties. Indeed, on the basis of our understanding of their structure and electronic properties, we have successfully designed an $Au_{25}(SR)_{18}$ catalyst for hydrogenation of ketones.[14] We are motivated to further study the $Au_n(SR)_m$ catalytic properties with a focus on some fundamental aspects of catalytic oxidation reactions, such as O_2 activation or effects of oxidants.

Herein, we choose the selective oxidation of styrene as a target in hope of gaining insight into the fundamentals of $Au_n(SR)_m$ catalysis and demonstrating the usefulness of such an atomic-level strategy in revealing the nanocatalysis from the perspective of $Au_n(SR)_m$ catalysts. We have devised two types of supported $Au_n(SR)_m$ ($R=CH_2CH_2Ph$) catalysts for selective oxidation of styrene by using hydroxyapatite (HAP, $Ca_{10}(PO_4)_6(OH)_2$) and SiO_2 supports. The remarkable catalytic activity of $Au_n(SR)_m$ nanoclusters is ascribed to their unique core–shell geometric and electronic structures.

Results and Discussion

In the target reaction of styrene oxidation, styrene contains a C=C double bond, which can be selectively oxidized to three products: benzaldehyde, styrene epoxide, and acetophenone. To elucidate the effects of size and atomic-packing architecture of gold nanoclusters and the effects of supports, $Au_n(SR)_m$ nanoclusters with molecular purity have been prepared and characterized in our previous work.[10–12] Herein, these nanoclusters are investigated for selective oxidation of styrene with various oxidants. We chose three oxidant systems: 1) TBHP (*tert*-butyl hydroperoxide) as the oxidant, 2) TBHP as an initiator and O_2 as the main oxidant, and 3) O_2 as the oxidant (without initiator).

We first discuss the catalytic activity of uncalcined $Au_n(SR)_m/SiO_2$ catalysts. Since the catalytic reaction temperature (80 °C) is below the thiolate-desorption onset temperature of $Au_n(SR)_m$ ($\approx$190 °C, Figure 1), we believe that the thiolate ligands should remain on the Au_n nanoclusters during the course of the catalytic reaction. Note that small molecules such as styrene can readily penetrate the thiolate ligand shell of $Au_n(SR)_m$ and reach the cluster surface where the catalytic reaction occurs.[14] We choose SiO_2 as the catalyst support in consideration of that it is generally inert (i.e., no electronic interaction with nanoparticles takes place) and thus, no major contribution to styrene oxidation occurs, and accordingly, one can study the intrinsic size-dependent catalytic properties of $Au_n(SR)_m$ nanoclusters. From Figure 2A, it is clearly observed that system 1 (i.e., TBHP as the oxi-

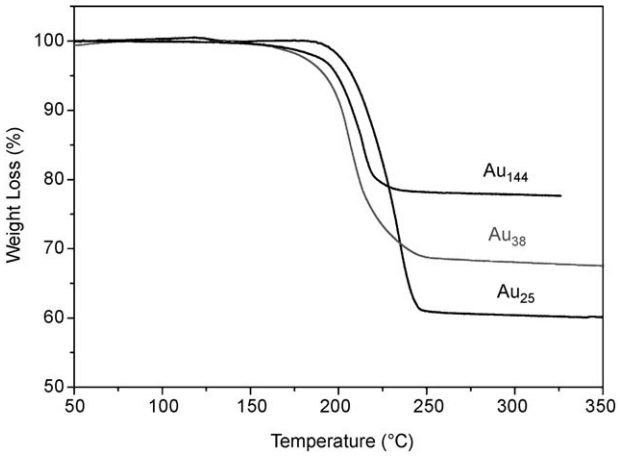

Figure 1. Thermogravimetric analysis (TGA) of $Au_{25}(SR)_{18}$, $Au_{38}(SR)_{24}$, and $Au_{144}(SR)_{60}$ nanoclusters ($R=CH_2CH_2Ph$).

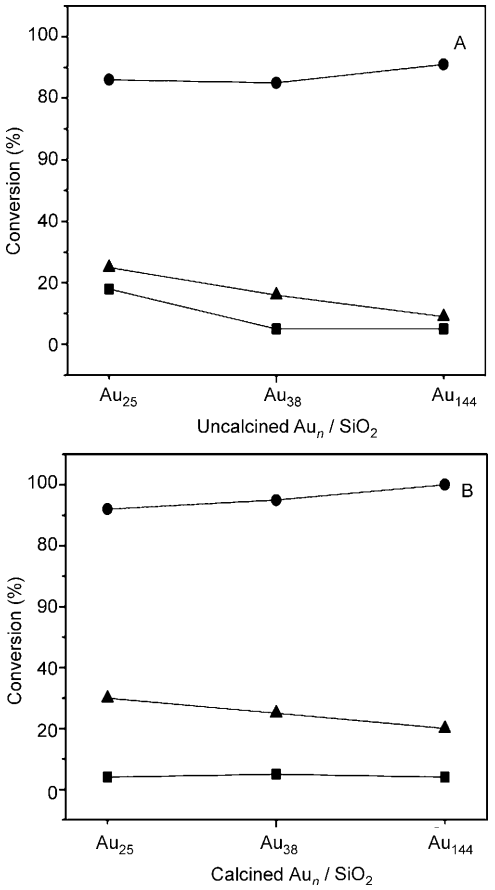

Figure 2. Catalytic activity of A) uncalcined $Au_n(SR)_m/SiO_2$ and B) at 200 °C calcined $Au_n(SR)_m/SiO_2$ catalysts for styrene oxidation. In each case, three systems are investigated: 1) TBHP as the oxidant (●), 2) TBHP as an initiator and O_2 as the main oxidant (▲), and 3) O_2 as the sole oxidant (■). Reaction conditions: 80 °C for 12 h in a toluene.

dant) gives the highest activity (e.g., 86% conversion to all products with $Au_{25}(SR)_{18}/SiO_2$ catalyst, ≈100% selectivity for benzaldehyde, see Figure S1 in the Supporting Information for selectivity), followed by system 2 (TBHP initiator/O_2 oxidant) that shows 25% activity (≈100% selectivity for benzaldehyde), and system 3 shows a somewhat lower activity (18% with $Au_{25}(SR)_{18}/SiO_2$, 80% selectivity for benzaldehyde). A similar order of activity was found for $Au_{38}(SR)_{24}/SiO_2$ and $Au_{144}(SR)_{60}/SiO_2$ catalysts in the three different oxidant systems (Figure 2A). Therefore, the constituent of the oxidant plays a critical role in the catalytic activity. TBHP is known to be highly reactive and hence, gives rise to the highest activity. When O_2 is used as the main or sole oxidant (systems 2 and 3, respectively), the activity significantly decreased, which indicates that O_2 activation is the key step for styrene oxidation. These results also imply that the active oxygen species in the catalytic cycles may be a peroxide-like surface species, since system 1 shows the highest activity.

In terms of the size effect, systems 2 and 3 show the following order of activity: $Au_{25} > Au_{38} > Au_{144}$ (Figure 2A), demonstrating that smaller $Au_n(SR)_m$ nanoclusters are more efficient in activating O_2 molecules, hence, show higher catalytic activity. But system 1 (with TBHP as oxidant) demonstrates that all three Au_n sizes show very high activity (> 85%), indicating that the activation of TBHP does not strongly depend on the size of the Au_n catalyst.

We have also investigated calcined $Au_n(SR)_m/SiO_2$ catalysts (calcination conditions: 200°C, 2 h). In this case, we expect the surface thiolate ligands to be partially desorbed, since the temperature is above the desorption onset temperature (Figure 1), hence, the Au_n nanocluster surfaces should become partially bare due to ligands loss, potentially giving rise to higher catalytic activity. On the negative side, since the SiO_2 support is inert and only weakly interacts with the nanoparticles, the partial loss of thiolate ligands may also lead to Au_n nanocluster agglomeration at 200°C (note that the catalytic reaction is performed at 80°C and should not result in further cluster aggregation in the course of the reaction); the resulting larger Au nanoparticles would be less catalytically active. Our results indeed indicate the positive and negative effects of the pretreatment of the catalyst at 200°C (Figure 2B). Compared with uncalcined catalysts, system 1 shows an increase of 6–10% in activity for the different sized $Au_n(SR)_m/SiO_2$ catalysts. System 2 shows an increase of 5–11%, but system 3 instead shows a drop in activity for all the $Au_n(SR)_m/SiO_2$ catalysts (e.g., 18% conversion with uncalcined $Au_{25}(SR)_{18}/SiO_2$ catalysts vs. 4% conversion with calcined catalysts). The observed activity loss in system 3 is apparently due to Au_n sintering during the 200°C pretreatment, which is not surprising since the O_2 activation in system 3 requires small nanoclusters but sintered particles can no longer effectively activate O_2. In contrast, in system 1, TBHP can readily be activated even with larger particles, hence, the increased accessibility of the catalyst surface due to partial removal of ligands leads to higher activity. Regarding system 2 (TBHP/O_2), we believe that O_2 attains activation and enters the catalytic cycle through interacting with the initial TBHP-induced peroxide-like species present on the gold surface, hence, even after the TBHP initiator is quickly consumed, O_2 can still drive the catalytic cycle and give rise to higher activity than system 3 (sole O_2). In system 3, without TBHP as the initiator the surface concentration of peroxide-like active species would be less, hence, lower catalytic activity is the consequence.

From the above-discussed difference between the TBHP-involved systems (1 and 2) and the sole O_2 system 3, we can infer that O_2 activation needs smaller Au particles such as $Au_{25}(SR)_{18}$, hence, a size dependence is observed, whereas TBHP activation can occur even with larger Au particles. This explains that the systems 1 and 2 (both involving TBHP) still show higher activity with the thermally pretreated catalysts (in which particle sintering occurs), but such catalysts show very low activity in system 3 (sole O_2) because larger particles can no longer activate O_2 in our experimental conditions.

The above-described catalytic results of $Au_n(SR)_m/SiO_2$ imply the importance of small particles in order to obtain high activity with O_2 or TBHP/O_2 as the oxidant. Herein, we introduce HAP oxide support. HAP is widely used in catalysis and has recently been investigated for gold nanocluster catalyst by Tsukuda et al.[9] In contrast to SiO_2, HAP is not inert. We expect that $Au_n(SR)_m$ could be stably adsorbed on a HAP surface and avoid sintering during the pretreatment at 200°C because of stronger interaction between $Au_n(SR)_m$ and the PO_4^{3-} moieties on HAP.[9,17]

The results of catalytic activity of the uncalcined and calcined $Au_n(SR)_m$/HAP catalysts for the three oxidant systems are shown in Figure 3 and their selectivity for benzaldehyde is shown in Figure S2 in the Supporting Information. The highest activity is again achieved in the TBHP oxidant system, since TBHP is more effective than O_2, (Figure 3A). The overall order of activity is TBHP (system 1) > TBHP/O_2 (system 2) > sole O_2 (system 3). Compared to the uncalcined catalysts, the calcined $Au_n(SR)_m$/HAP catalysts (Figure 3B) show a considerable increase in activity for the systems 1 and 2 (but not for system 3). System 1 (TBHP as oxidant) gives ≈100% conversion of styrene for all three sizes of catalysts. System 2 shows 8–14% increase in conversion, but system 3 has a large drop (10–18%) in activity due to moderate Au_n sintering and larger Au particles being incapability of activating O_2. With HAP as the support, a size effect is also observed, that is, smaller $Au_n(SR)_m$ clusters exhibit higher catalytic activity.

Overall, the trends observed in the HAP-supported catalysts are similar to the SiO_2-supported catalysts, including that the oxidant systems involving TBHP show higher conversion of styrene than the sole O_2 system, and that O_2 activation needs small clusters but TBHP can be activated even with large Au particles. However, a large difference between SiO_2- and HAP-supported catalysts is that $Au_n(SR)_m$/HAP catalysts are generally more active than $Au_n(SR)_m/SiO_2$ catalysts, in particular in system 2 (TBHP/O_2), in which a ≈20% increase in activity was observed for both uncalcined (see

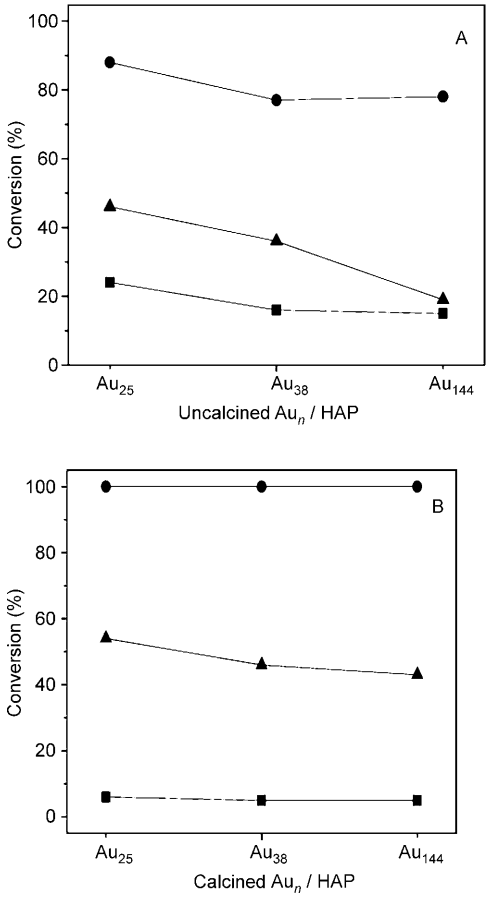

Figure 3. Catalytic activity of A) uncalcined $Au_n(SR)_m$/HAP and B) calcined $Au_n(SR)_m$/HAP catalysts for styrene oxidation. In each case, three oxidant systems are investigated: 1) TBHP as the oxidant (●), 2) TBHP as an initiator and O_2 as the main oxidant (▲), and 3) O_2 as the sole oxidant (■). Reaction conditions: 80 °C for 12 h in a toluene.

Figures 2A and 3A) and calcined catalysts (see Figures 2B and 3B). Note that control experiment shows that HAP itself does not catalyze styrene oxidation under comparable conditions. The results imply that HAP, to some extent, stabilizes $Au_n(SR)_m$ nanoparticles and the electronic interaction between HAP and $Au_n(SR)_m$ leads to large increase in catalytic activity of $Au_n(SR)_m$/HAP catalysts compared to $Au_n(SR)_m/SiO_2$ catalysts. The stabilization of the nanoclusters by HAP is evidenced by no color change of the catalyst before and after thermal treatment and also by TEM imaging (Figure S3 in the Supporting Information). In addition, when one compares calcined catalysts with uncalcined ones (Figure 3A and B), the calcined catalysts show higher activity due to partial removal of surface ligands, similar to the conclusion from the $Au_n(SR)_m/SiO_2$ catalysts.

To compare the catalytic results in a different perspective, Figure S4–S6 in the Supporting Information show the catalytic results of different catalysts corresponding to the same oxidant system 1, 2, or 3. In all three oxidant systems, HAP as a support to immobilize $Au_n(SR)_m$ is always much more effective than inert SiO_2 as support. When TBHP is used as the oxidant (i.e., system 1), the calcined $Au_n(SR)_m$ catalysts can achieve higher activity than the uncalcined $Au_n(SR)_m$ catalysts (Figure S4 in the Supporting Information). When TBHP is used as an initiator and O_2 as the main oxidant (i.e., system 2), in addition to the trend that calcined $Au_n(SR)_m$ catalysts show higher activity than the uncalcined catalysts, one also observes that the smaller the size of $Au_n(SR)_m$, the higher the activity (Figure S5 in the Supporting Information). In system 3 (sole O_2 as the oxidant), unlike systems 1 and 2, the uncalcined $Au_n(SR)_m$ catalysts achieve higher activity than the calcined $Au_n(SR)_m$ catalysts (Figure S6 in the Supporting Information). This is due to cluster sintering in calcination and the resultant larger particles cannot effectively activate O_2.

We have also investigated the recyclability of the supported $Au_n(SR)_m$ catalysts. In this test, the supported $Au_n(SR)_m$ catalysts were recovered after the reaction was completed and then reused in a new run under identical reaction conditions. As shown in Figures 4, 5, and 6 (corresponding to oxidant systems 1, 2, and 3, respectively), all the $Au_n(SR)_m$ catalysts supported on HAP or SiO_2 only show a slight decrease in activity after multiple cycles, and no loss of selectivity was observed.

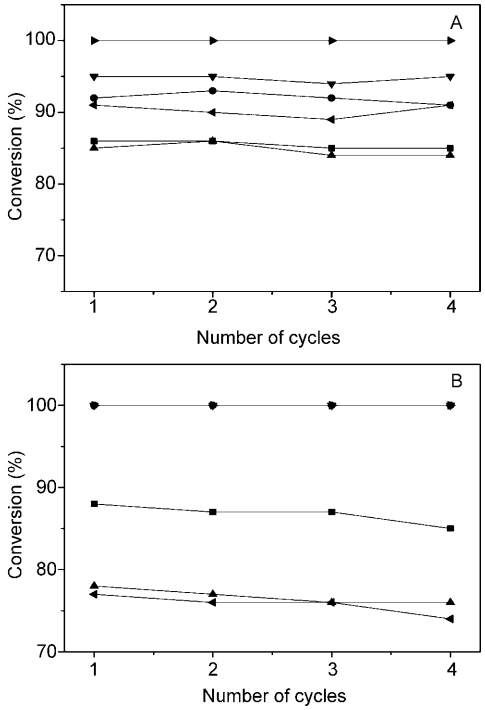

Figure 4. Recyclability of A) $Au_n(SR)_m/SiO_2$ and B) $Au_n(SR)_m$/HAP catalysts for styrene oxidation with TBHP as the oxidant system (■ = uncalcined supported Au_{25}, ● = calcined supported Au_{25}, ▲ = uncalcined supported Au_{38}, ▼ = calcined supported Au_{38}, ◀ = uncalcined supported Au_{144}, and ▶ = calcined supported Au_{144}).

The above results on the catalytic styrene oxidation by $Au_n(SR)_m$ allow to gain some valuable insight into gold nanocatalysis at the atomic level. In the catalytic reaction, the Au_n cluster as an entity serves as the active species. The

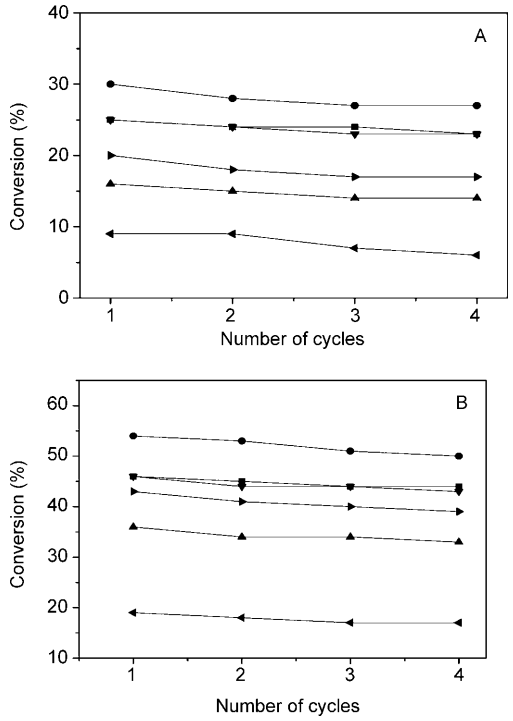

Figure 5. Recyclability of A) $Au_n(SR)_m/SiO_2$ and B) $Au_n(SR)_m$/HAP catalysts for styrene oxidation with TBHP as initiator and O_2 as the main oxidant system (■ = uncalcined supported Au_{25}, ● = calcined supported Au_{25}, ▲ = uncalcined supported Au_{38}, ▼ = calcined supported Au_{38}, ◀ = uncalcined supported Au_{144}, and ▶ = calcined supported Au_{144}).

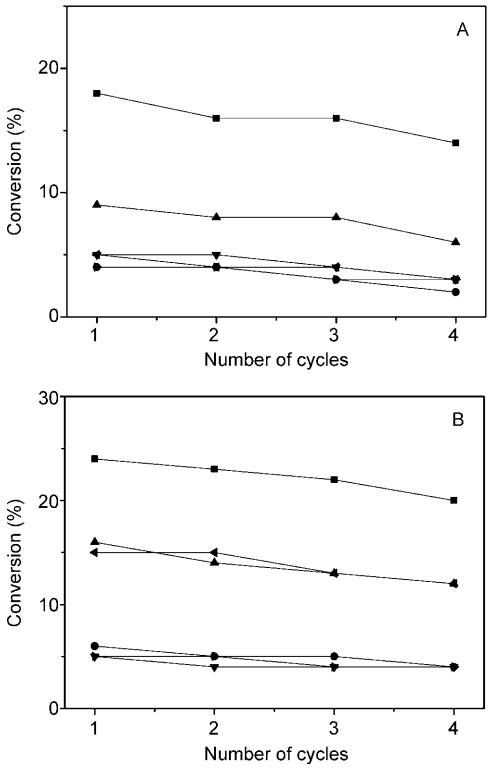

Figure 6. Recyclability of A) $Au_n(SR)_m/SiO_2$ and B) $Au_n(SR)_m$/HAP catalysts for styrene oxidation with O_2 as the sole oxidant system (■ = uncalcined supported Au_{25}, ● = calcined supported Au_{25}, ▲ = uncalcined supported Au_{38}, ▼ = calcined supported Au_{38}, ◀ = uncalcined supported Au_{144}, and ▶ = calcined supported Au_{144}).

unique properties of small Au_n nanoclusters, including non-fcc atomic packing structure and core–shell-type electronic properties[10] are believed to have a strong impact on the catalytic activity. Herein, we choose Au_{25} as a model for a detailed discussion since we have solved its crystal structure, including its anionic and charge-neutral states. The crystal structures of $[Au_{25}(SR)_{18}]^q$ ($q = -1$, 0) show a core–shell structure consisting of an Au_{13} icosahedral core and an exterior Au_{12} shell (Figure 7).[10,21] The charge distribution on the Au_{13} core and the Au_{12} shell is quite different:[10,18–20] the Au_{13} core possesses eight ($q = -1$) or seven ($q = 0$) delocalized valence electrons. These electrons originate from Au(6s) and are primarily distributed within the Au_{13} core, whereas the Au_{12} shell bears positive charges due to bonding of thiolates and electron transfer from gold to sulfur of the thiolate ligands. The electron-rich Au_{13} core should facilitate O_2 activation by electron transfer to O_2, accompanied by oxidative conversion of $[Au_{25}(SR)_{18}]^-$ into neutral $[Au_{25}(SR)_{18}]^0$ (see Figure 7).[19,21] The conversion between the anionic and neutral $Au_{25}(SR)_{18}$ nanoclusters is completely reversible by using peroxide or O_2 as the oxidant (Figure 7). This redox property of $Au_{25}(SR)_{18}$ should be primarily responsible for O_2 activation and subsequently for the catalytic oxidation of styrene.

Here, we propose a mechanism for selective oxidation of styrene catalyzed by $Au_{25}(SR)_{18}$ nanoclusters (Scheme 1). The three different oxidant systems can undergo different reaction pathways to activate the oxidants and generate a

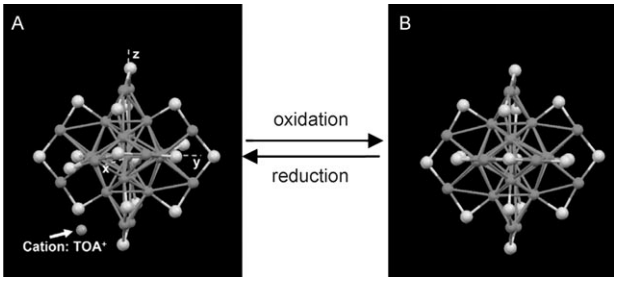

Figure 7. Reversible conversion between the anionic and neutral $Au_{25}(SR)_{18}$ clusters and the crystal structures of anionic (A) and neutral (B) $Au_{25}(SR)_{18}$ clusters (TOA^+ = tetraoctylammonium).

common peroxyformate intermediate Au_{25}–$O_{2(ad)}$ (species D): 1) in the case of TBHP as the oxidant, interaction of TBHP and anionic Au_{25} (species A) forms a hydroperoxy species B, and then species B loses a H_2O molecule and rearranges to give rise to the Au_{25}–$O_{2(ad)}$ species D. 2) In the case of TBHP/O_2, initiation of TBHP forms species BuO•/•OH,[22,23] which activates dioxygen to form the superoxo-like $O_2^{\bullet}$ (formally O_2^-), in which the intermediate has been verified previously in computations of Au_n-catalyzed CO oxidation in liquid phase[24] and in gas phase.[25] The superoxo-like $O_2^{\bullet}$ is adsorbed in a side-on fashion to the gold surface with two partial Au–O bonds to produce a low-barrier tran-

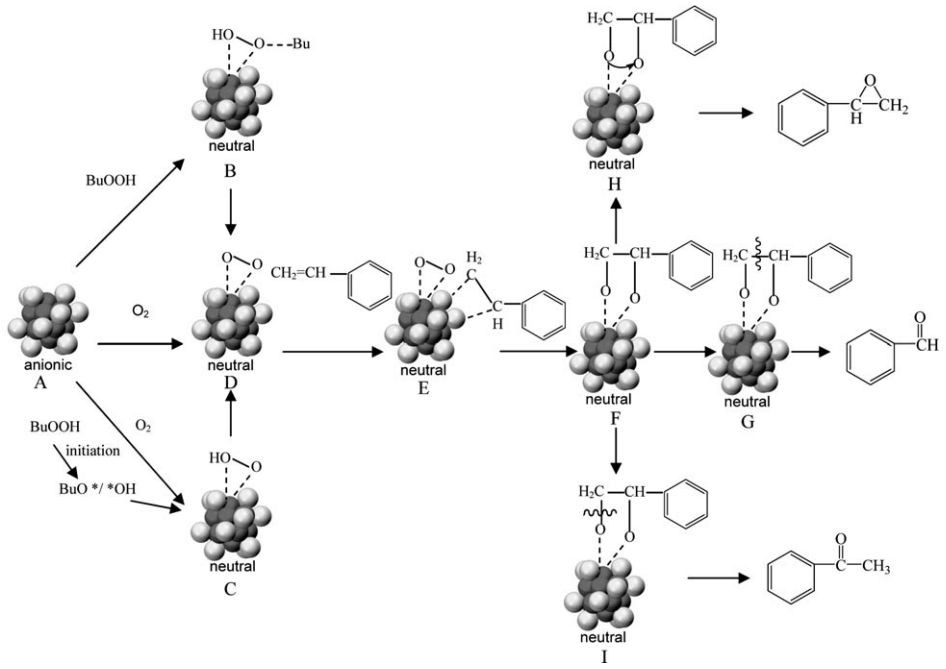

Scheme 1. Proposed mechanism of selective oxidation of styrene catalyzed by a $Au_{25}(SR)_{18}$ cluster. For clarity, the thiolate ligands are not shown. (Dark gray: Au atoms of the core, light gray: Au atoms of the shell).

sition state species C, and then the peroxo-like species C transforms to the Au_{25}–$O_{2(ad)}$ species D. 3) In the case of sole O_2 as oxidant, O_2 directly attacks the Au_{13} core[26] to form the Au_{25}–$O_{2(ad)}$ species D.

The above-described processes pertain to O_2 activation and primarily involve the electron-rich Au_{13} core of the Au_{25} particle. With respect to C=C activation of styrene, the presence of partial positive charges on the surface gold atoms ($Au^{\delta+}$, $\delta \approx 0.3$) of the Au_{12} shell should greatly facilitate activation of the nucleophilic $-CH=CH_2$ group in styrene (species E) since the positive Au atoms on the shell are electrophilic. Then the activated C=C bond reacts with the $O_{2(ad)}$ species through side-by-side interaction (or π–π bonding) on the Au_{25} surface, leading to species F. Subsequently, the catalytic selectivity is triggered by the dissociation and rearrangement in three competing pathways that lead to the three products: the formation of benzaldehyde from the breaking of the C–C bond (species G), the epoxide is created by the transfer of oxygen to the olefinic bond to form a metalloepoxy intermediate (species H), and acetophenone is produced by the breaking of the C–O bond (species I). From the experimental results (Figures S1 and S2 in the Supporting Information), the selectivity for benzaldehyde is much higher than that for the other two products, implying that the competing pathway to form benzaldehyde is favored on the Au_n nanocluster catalysts, which is also supported by a recent DFT study.[27] Finally, the oxidized catalyst, $[Au_{25}(SR)_{18}]^0$, can be reduced to the anionic form $[Au_{25}(SR)_{18}]^-$ by gaining an electron when the C=C bond leaves the Au_{25} cluster, hence, one catalytic cycle is completed.

Note, that the core–shell structure of neutral $Au_{25}(SR)_{18}$ is almost identical with the anionic $Au_{25}(SR)_{18}$ (Figure 7), so both of them can act as the active catalysts to activate the oxidant and the C=C bond. The structures of $Au_{38}(SR)_{24}$ and $Au_{144}(SR)_{60}$ have recently been computed by theoretical calculations.[28,29] The atom packing structure of $Au_{38}(SR)_{24}$ was predicted to be based on a face-fused biicosahedral Au_{23} core (i.e., $13+13-3=23$, D_{3h} symmetry). The Au_{23} core is further structurally strengthened by three -S(*R*)-Au-S(*R*)- monomeric "staples" distributed at the waist of Au_{23} and six "V"-shaped -S(*R*)-Au-S(*R*)-Au-S(*R*)- dimeric staples evenly distributed on the two icosahedral units of Au_{23}. The $Au_{144}(SR)_{60}$ nanocluster was predicted to have an icosahedral symmetry and to consist of a core of 114 Au atoms arranged into three concentric shells of 12, (30+12), and 60 symmetry-equivalent atoms.[29] Overall, the catalytic activity of $Au_n(SR)_m$ nanoclusters can be explained by their core–shell-type geometric and their electronic structures, similar to the proposed mechanism as shown in Scheme 1.

It is worth commenting that, when O_2 is used as the oxidant, a distinct size effect is observed for Au_n catalysts in selective oxidation of styrene, with the order of catalytic activity: $Au_{25} > Au_{38} > Au_{144}$. Their ultrasmall size is primarily responsible for the catalytic activity observed in styrene oxidation. The experimental result is echoed by theoretical studies,[24,30] which demonstrate a sharp size threshold (<2 nm) in catalytic activity for CO oxidation catalyzed by Au_n clusters,[24] and a similar size threshold for O_2 dissociation on Au_n clusters.[30] The sizes of $Au_{25}(SR)_{18}$, $Au_{38}(SR)_{24}$, and $Au_{144}(SR)_{60}$ are 0.98, 1.3, and 1.6 nm, respectively. The ultrasmall size of these Au nanoparticles is comparable to the de Broglie wavelength of conduction electrons, hence, quantum confinement effects lead to drastically altered electronic structure in these ultrasmall particles. The $Au_{25}(SR)_{18}$ and $Au_{38}(SR)_{24}$ nanoclusters exhibit large HOMO–LUMO gaps in their electronic structures: $E_g(Au_{25}) \approx 1.3$ and $E_g(Au_{38}) \approx 0.9$ eV.[10–13] Of note, no distinct HOMO–LUMO gap was found in $Au_{144}(SR)_{60}$, but the cluster is still nonmetallic because the surface plasmon resonance at ≈520 nm is absent in the cluster.[12c] We believe that the catalytic mechanism proposed for Au_{25} (Scheme 1) should be valid for Au_{38} and Au_{144} nanocluster catalysts. More details remain to be developed when a full understanding of their geometric and electronic structures are attained. Overall,

the particle-size-dependent catalytic performance of Au_{25}, Au_{38}, and Au_{144} is related to their quantum confinement effects. The ultrasmall size of these nanoclusters leads to electron energy quantization, in contrast with the quasi-continuous electronic band structure in large nanoparticles (>3 nm), for the latter, the collective electronic excitation (i.e., plasmon excitation) is observed.

Conclusion

The atomic-level strategy adopted in this work has provided important insight into the origin of Au catalysis from the perspective of monodisperse $Au_n(SR)_m$ nanoclusters. We found that dioxygen activation is the key step for selective oxidation of styrene. Small Au_n nanoclusters are capable of activating O_2, and HAP is found to facilitate O_2 activation by stabilizing Au_n on support surface and electronically interacting with the nanocluster. TBHP activation is facile and can be achieved even with larger Au nanoparticles and thus, does not show distinct size effect of Au_n. With more complete knowledge of the geometric and electronic structure information of $Au_n(SR)_m$ nanoclusters that will be revealed in future progress, one will ultimately be able to gain a full understanding of the origin of nanogold catalysis. These atomically monodisperse $Au_n(SR)_m$ catalysts are promising in that they will not only provide new opportunities for studying nanocatalysis at an atomic level, but also promote the development of a new generation of nanogold catalysts for real-world applications. The $Au_n(SR)_m$ catalysts are expected to bridge the gap between the model catalysts and realistic catalytic applications.

Experimental Section

Characterization: NMR (^{1}H NMR) spectra were measured on a Bruker Avance 300 MHz. GC mass spectra were obtained by using a Thermo Finnigan Trace GC 2000 and an Rxi-XLB chromatographic column. TEM imaging was performed on a Hitachi 7100 microscope operated at 75 kV.

Preparation of $Au_{25}(SCH_2CH_2Ph)_{18}$:[11] $HAuCl_4{\cdot}3H_2O$ (0.4 mmol) dissolved in nanopure water (5 mL), and tetraoctylammonium bromide (TOAB, 0.47 mmol) dissolved in toluene (10 mL), were combined in a 25 mL three-neck round bottom flask. The solution was vigorously stirred with a magnetic stir bar to facilitate phase transfer of gold(III) salt into the toluene phase. After 15 min, phase transfer was completed, leaving a clear aqueous phase at the bottom of the flask, then the aqueous layer was removed by using a 10 mL syringe. The toluene solution of gold(III) was purged with N_2 and cooled down to 273 K in an ice bath over a period of 30 min under magnetic stirring. $PhCH_2CH_2SH$ (0.17 mL) was added. The deep-red solution turned to faint yellow over a period of 5 min, and finally to clear over 1 h. After the solution turns to clear, an aqueous solution of $NaBH_4$ (6 mL, 4 mmol) was quickly added. The reaction was allowed to proceed overnight under N_2 atmosphere. Ethanol (20 mL) was added to separate Au_{25} clusters from TOAB. The Au_{25} clusters were collected after removing the supernatant. The Au_{25} clusters were extracted with acetonitrile.

Preparation of $Au_{38}(SCH_2CH_2Ph)_{24}$:[12b] $HAuCl_4{\cdot}3H_2O$ (0.5 mmol) and glutathione (GSH, 2.0 mmol) were mixed in acetone (20 mL) at room temperature under vigorous stirring. The mixture was then cooled to 273 K in an ice bath for about 20 minutes. $NaBH_4$ (5 mmol, dissolved in cold nanopure water; 6 mL) was rapidly added to the suspension under vigorous stirring. After about 20 minutes, black $Au_n(SG)_m$ nanoclusters were found to precipitate out of solution and were deposited onto the inner wall of the flask. The clear acetone solution was decanted and water (6 mL) was added to dissolve the $Au_n(SG)_m$ clusters. A solution of $Au_n(SG)_m$ (around 200–300 mg, dissolved in nanopure water; 6 mL) was mixed with ethanol (0.3 mL), toluene (2 mL) and $PhCH_2CH_2SH$ (2 mL). The solution was heated to 353 K in air and allowed to react for about 40 hrs. Over the long etching process, the initial polydisperse Au_n nanoclusters were finally converted to monodisperse $Au_{38}(SCH_2CH_2Ph)_{24}$ clusters. Excess ethanol was used to precipitate the Au clusters. The $Au_{38}(SCH_2CH_2Ph)_{24}$ clusters were extracted with toluene.

Preparation of $Au_{144}(SCH_2CH_2Ph)_{60}$:[12c] A solution of TOAB (0.116 mmol) in toluene (20 mL) was mixed with an aqueous solution of $HAuCl_4{\cdot}3H_2O$ (0.1 mmol, 20 mL). After phase transfer of gold(III) into toluene, the aqueous layer was removed. $PhCH_2CH_2SH$ (1.5 mmol) was added, followed by stirring for 30 min. The mixture was then cooled to 0 °C. $NaBH_4$ (0.1 mmol) in nanopure water (20 mL) of 0 °C was rapidly injected into the solution under vigorous stirring. After stirring the reaction mixture overnight, the organic phase was washed thoroughly with water and then the solvents were removed in vacuum. The residue was washed with methanol to remove excess $PhCH_2CH_2SH$, TOAB, and other byproducts. The dried samples ($\approx$20 mg) were incubated in pure $PhCH_2CH_2SH$ at 80 °C for 24 h under vigorous stirring. The final solution was washed thoroughly with methanol and then acetone to remove byproducts such as gold(I)–$PhCH_2CH_2SH$ complexes. The $Au_{144}(SCH_2CH_2Ph)_{60}$ clusters were extracted from the products with toluene.

Preparation of supported $Au_n(SR)_m$ catalysts: The SiO_2-supported $Au_n(SR)_m$ clusters were obtained by stirring a solution of Au clusters in dichloromethane with a calculated amount of SiO_2 (fumed, 0.014 μm, (200 ± 25) m^2g^{-1}) for one day and the solution was removed in flowing nitrogen. In an analogous preparation of another Au_n/SiO_2 sample, in vacuo thermal treatment (473 K, 2 h) was required. The preparation of HAP-supported $Au_n(SR)_m$ is similar with that of SiO_2-supported $Au_n(SR)_m$.

The catalysts test

TBHP as an oxidant: Supported gold catalysts (100 mg powder, 1 %wt loading of Au) were mixed with styrene (90 μL), TBHP (0.5 mL) and toluene (20 mL) in a 50 mL sealed glass reactor with vigorous stirring. Then the mixture was heated to 353 K for 12 h.

O_2 as an oxidant: A 50 mL sealed glass reactor loaded with supported gold catalyst (100 mg powder, 1 %wt loading of Au), styrene (90 μL), and toluene (20 mL) was filled with dioxygen stream (99.995 %, Messer). After purging to remove air the mixture was vigorous stirred and heated to 353 K for 12 h.

TBHP as an initiator and O_2 as an oxidant: A 50 mL sealed glass reactor loaded with supported gold catalyst (100 mg powder, 1 %wt loading of Au), styrene (90 μL), TBHP (7.2 μL), and toluene (20 mL) was filled with dioxygen stream (99.995 %, Messer). After purging to remove air the mixture was stirred vigorously, and heated to 353 K for 12 h. The products were analyzed by ^{1}H NMR spectroscopy and GC-MS. The conversion and selectivity were calculated from quantitative NMR spectroscopy. The error is ±1 %.

Acknowledgements

We acknowledge financial support from CMU, AFOSR, and NIOSH.

[1] T. Hayashi, K. Tanaka, M. Haruta, *J. Catal.* **1998**, *178*, 566–575.
[2] A. S. K. Hashmi, G. J. Hutchings, *Angew. Chem.* **2006**, *118*, 8064–8105; *Angew. Chem. Int. Ed.* **2006**, *45*, 7896–7936.
[3] A. Corma, H. Garcia, *Chem. Soc. Rev.* **2008**, *37*, 2096–2126.

[4] J. Guzman, B. C. Gate, *J. Am. Chem. Soc.* **2004**, *126*, 2672–2673.
[5] J. C. F. Gonzales, B. C. Gates, *Chem. Soc. Rev.* **2008**, *37*, 2127–2134.
[6] Y. Liu, H. Tsunoyama, T. Akita, T. Tsukuda, *J. Phys. Chem. C* **2009**, *113*, 12457–13461.
[7] M. Turner, V. B. Golovko, O. P. H. Vaughan, P. Abdulkin, A. B. Murcia, M. S. Tikhov, B. F. G. Johnson, R. M. Lambert, *Nature* **2008**, *454*, 981–983.
[8] Y. Zhu, H. Qian, M. Zhu, R. Jin, *Adv. Mater.* **2010**, *22*, 1915–1920.
[9] Y. Liu, H. Tsunoyama, T. Akita, T. Tsukuda, *Chem. Commun.* **2010**, *46*, 550- 552.
[10] M. Zhu, C. M. Aikens, F. J. Hollander, G. C. Schatz, R. Jin, *J. Am. Chem. Soc.* **2008**, *130*, 5883–5885.
[11] M. Zhu, E. Lanni, N. Gary, M. E. Bier, R. Jin, *J. Am. Chem. Soc.* **2008**, *130*, 1138–1139.
[12] a) H. Qian, M. Zhu, U. N. Andersen, R. Jin, *J. Phys. Chem. A* **2009**, *113*, 4281–4284; b) H. Qian, Y. Zhu, R. Jin, *ACS Nano* **2009**, *3*, 3795–3803; c) H. Qian, R. Jin, *Nano Lett.* **2009**, *9*, 4083–4087.
[13] N. K. Chaki, Y. Negishi, H. Tsunoyama, Y. Shichibu, T. Tsukuda, *J. Am. Chem. Soc.* **2008**, *130*, 8608–8610.
[14] Y. Zhu, H. Qian, B. A. Drake, R. Jin, *Angew. Chem.* **2010**, *122*, 1317–1320; *Angew. Chem. Int. Ed.* **2010**, *49*, 1295–1298.
[15] A. Lyalin, T. Taketsugu, *J. Phys. Chem. C* **2009**, *113*, 12930–12934.
[16] W. Gao, X. F. Chen, J. C. Li, Q. Jiang, *J. Phys. Chem. C* **2010**, *114*, 1148–1153.
[17] K. Mori, T. Hara, T. Mizugaki, K. Ebitani, K. Kaneda, *J. Am. Chem. Soc.* **2004**, *126*, 10657–10666.
[18] J. Akola, M. Walter, R. L. Whetten, H. Hakkinen, H. Gronbeck, *J. Am. Chem. Soc.* **2008**, *130*, 3756–3757.
[19] M. Zhu, C. M. Aikens, M. P. Hendrich, R. Gupta, H. Qian, G. C. Schatz, R. Jin, *J. Am. Chem. Soc.* **2009**, *131*, 2490–2492.
[20] C. M. Aikens, *J. Phys. Chem. C* **2008**, *112*, 19797–19800.
[21] M. Zhu, W. T. Eckenhoff, T. Pintauer, R. Jin, *J. Phys. Chem. C* **2008**, *112*, 14221–14224.
[22] M. D. Hughes, Y. Xu, P. Jenkins, P. Mcmorn, P. Landon, D. I. Enache, A. F. Carley, G. A. Attard, G. J. Hutchings, F. King, E. H. Stitt, P. Johnston, K. Griffin, C. J. Kiely, *Nature* **2005**, *437*, 1132–1135.
[23] P. Lignier, F. Morfin, S. Mangematin, L. Massin, J. Rousset, V. Caps, *Chem. Commun.* **2007**, 186–188.
[24] O. L. Acevedo, K. A. Kacprzak, J. Akola, H. Häkkinen, *Nat. Chem. Biol.* **2010**, *6*, 329–334.
[25] L. D. Socaciu, J. Hagen, T. M. Bernhardt, L. Woste, U. Heiz, H. Häkkinen, U. Landman, *J. Am. Chem. Soc.* **2003**, *125*, 10437–10445.
[26] M. Okumura, Y. Kitagawa, M. Haruta, K. Yamaguchi, *Appl. Catal. A* **2005**, *291*, 37–44.
[27] Y. Pei, N. Shao, Y. Gao, X. C. Zeng, *ACS Nano* **2010**, *4*, 2009–2020.
[28] Y. Pei, Y. Gao, X. C. Zeng, *J. Am. Chem. Soc.* **2008**, *130*, 7830–7832.
[29] O. Lopez-Acevedo, J. Akola, R. L. Whetten, H. Grönbeck, H. Häkkinen, *J. Phys. Chem. C* **2009**, *113*, 5035–5038.
[30] A. Roldán, S. Gonzalez, J. M. Ricart, F. Illas, *ChemPhysChem* **2009**, *10*, 348–351.

Received: April 23, 2010
Published online: August 16, 2010

